Hindawi
Geofluids
Volume 2022, Article ID 1795369, 13 pages
https://doi.org/10.1155/2022/1795369

Research Article

Well Interference Analysis of Shale Gas Wells Based on Embedded Discrete Fracture Model

Qing Zhang

Shale Gas Exploration and Development Department, CNPC Chuanqing Drilling Engineering Co., Ltd., Chengdu, Sichuan 610051, China

Correspondence should be addressed to Qing Zhang; zhangpetro@126.com

Received 16 November 2021; Accepted 15 January 2022; Published 19 April 2022

Academic Editor: Shuyang Liu

Well interference is commonly observed in shale gas reservoirs due to the small well spacing, and it significantly affects the shale gas production. Effective evaluation of well interference is important to increase the gas production of shale gas wells. Previous researches mainly focus on the well interference phenomenon and production optimization using numerical simulation so that the quantitative analysis of shale gas well interference is rare. Therefore, this paper is aimed at analyzing the well interference of shale gas wells through production type curves. First, the complex fracture networks are described by using the embedded discrete fracture model (EDFM). Second, different cases are designed to characterize different types and degrees of well interference in shale gas reservoirs. Third, numerical modelling is conducted to simulate the well interference and its effect on gas production. Fourth, the type curves are obtained to quantitatively analyze and compare the impact of well interference on shale gas production. Results show that well interference caused by hydraulic fractures mainly reduce the gas production of the parent well while the gas production of child well can be increased owing to the larger equivalent stimulated area. The pressure depletion is obvious when the well communication degree becomes higher. Differences can be found from early to late periods by the combination of log-log and Blasingame type curves. This work provides a method for well interference evaluation, and it can be used to obtain well spacing and adjust fracturing parameter in shale gas reservoirs.

1. Introduction

The permeability and porosity of shale gas reservoirs are ultralow due to abundant nanopores [1–5]. Stimulation technology is required to obtain commercial productivity [6]. Horizontal well drilling and hydraulic fracturing technologies have been commonly used to generate high-permeability fracture networks [7–11]. Multiwell pad is further introduced to decrease the drilling and fracturing costs, and each well pad is usually composed of six to eight horizontal wells [12, 13]. However, well interference is observed in shale gas reservoirs due to the small well spacing (e.g., 300 m to 500 m). How to characterize and analyze the well performance in shale gas reservoirs is important for enhancing the ultimate shale gas production [14].

In recent years, the well interference phenomena in unconventional oil and gas reservoirs have attracted much research interest [15–17]. The well interference is modelled using different methods. Lawal et al. simulated and forecasted frac hits in shale gas wells and indicated that the gas production reduction was caused by the flow resistance due to the multiphase flow in the fracture network or the permeability decrease around the wells [18]. Moradi and Angus modelled the frac hits by using dynamic microseismicity-constrained enhanced fracture regions [19]. Guo et al. conducted numerical investigation about the effects of subsequent parent well injection on interwell fracturing interference using reservoir-geomechanics-fracturing modelling approaches [20]. Mohaghegh presented dynamic simulation of frac hit based on artificial intelligence and machine learning methods [21]. The impact of fracturing interference on gas production performance is also analyzed [22]. The mechanisms of well interference and different types of well interference types in shale reservoirs are further investigated [23–25]. Various methods are developed to evaluate the well interference caused by hydraulic fracturing in the shale reservoirs. Sardinha et al.

applied frac pressure hits and production interference analysis to estimate the well connectivity [26]. Gupta et al. focused on identifying the well interference by forecasting long-term production and residual analysis [27]. Molina established an analytical model to assess the fraction of frac fits in multiwell pads [28]. Kumar et al. performed integrated analysis of tracer and pressure-interference tests to identify well interference [29]. Arman et al. forecasted the mid and far field frac hits at an Eagle Ford and Wolfcamp well based on shale pressure depletion and well performance using geomechanical constraints [30]. GIS Platform was used to evaluate the risks of frac hits in the Aishwarya Barmer-Hill Field [31]. Magneres et al. developed a workflow to estimate the well interferences and its maximum expected well head pressure using magnitude forecast methodology [32]. To enhance the shale gas production, well spacing needs to be optimized to decrease well interference [33–35]. Except for well spacing, the stimulation design also needs to be optimized [36]. Different fracturing technologies are applied to prevent well interference, including fracture geometry control technology [37] and adaptive fracturing [38]. Other prevention methods are also proposed to mitigate the well interference especially the frac hits, including preloading depleted parent wells or fluid injection [39–41], chemical or mechanical treatments such as refracturing or solvent/surfactant chemistry blend [42–44]. Also, there are some filed case studies about the mitigation measures for well interference [45, 46]. However, the remedial costs are huge and the recovering effect is uncertain by the prevention measures. A quick and accurate evaluation of well interference is important for selecting measures to reduce the effect of well interference on shale gas production. Exact characterization of complex fracture networks is required for shale gas wells, especially for the multiple wells with fracture interference [47–49]. The embedded discrete fracture model (EDFM) is able to accurately and efficiently deal with both natural fractures and hydraulic fractures, which does not require local grid refinement nearby fractures through nonneighboring connections [50–53]. PTA and RTA are methods to analyze well interference, which can identify the characteristics of well interference in some specific periods [54–59].

The current research mainly focuses on the phenomenon, reason, mechanism, and mitigation suggestions for well interference. The quantitative analysis method for shale gas well interference evaluation needs to be further investigated. Thus, this paper tries to analyze the well interference of shale gas wells through production type curves based on numerical simulation using EDFM technology.

2. Fracture Characterization and Calculation

Complex fracture networks are generated through large-scale hydraulic fracturing in shale gas formations. How to characterize and calculate the formed fracture networks including both hydraulic and natural fractures becomes a crucial issue for efficient development of shale gas resources. The dual porosity and dual permeability models belong to the continuum media, which is unavailable for the fracture description in shale gas reservoirs [60]. A discrete fracture model is more accurate to characterize the hydraulic fractures and natural fractures [61]. Although the discrete fracture model based on unstructured grids shows good performance in representing complex fracture geometries, the huge number of grids and big differences among grid scale result in high computation costs and poor convergence as well as difficulty on gridding [62]. Therefore, it is hard to efficiently handle the complex fractures by using the discrete fracture model based on unstructured grids. In recent years, the EDFM was developed to meet the accuracy of discrete fracture models with structured gridding especially in the unconventional oil and gas reservoirs [63]. The grid number is significantly reduced since the refinement near the fractures is not required compare to the discrete fracture model with unstructured gridding. Furthermore, the gridding is easier and the convergence is better based on EDFM.

2.1. Nonneighboring Connections. The nonneighboring connections (NNCs) are proposed to handle the different intersections among natural fractures, hydraulic fractures, and matrices [62]. The fracture can be divided into multiple segments through matrix cells and generate NNCs. The fluid flow between the fracture and matrix can be efficiently modelled using the transmissibility of NNCs [63].

The NNCs can be divided into three categories (see Figure 1), including the connection between the matrix grid and fracture segment, connection between different fracture segments within the same fracture, and connection between different fractures.

2.1.1. Transmissibility of Connection between Matrix Grid and Fracture Segment. The schematic of fracture-matrix connection can be found in Figure 1(a). Its transmissibility can be calculated by [62]

$$T_{f-m} = \frac{2A_f(\overrightarrow{\overrightarrow{K}} * \overrightarrow{n}) * \overrightarrow{n}}{d_{f-m}}, \tag{1}$$

$$d_{f-m} = \frac{\int_V X_n dV}{V}, \tag{2}$$

where A_f is the area of the fracture plane. $\overrightarrow{\overrightarrow{K}}$ denotes the permeability tensor. $\overrightarrow{n}$ is the normal vector of the fracture plane. d_{f-m} represents the distance between the matrix and fracture segment. V means the fracture volume. X_n denotes the distance from the matrix unit to the fracture segment.

2.1.2. Transmissibility of Connection between Fracture Segments within the Same Fracture. The connection between fracture segments from the same fracture is shown in Figure 1(b). Its transmissibility can be obtained and expressed as [62]

$$T_{\text{seg}} = \frac{T_1 T_2}{T_1 + T_2}, \tag{3}$$

$$T_1 = \frac{k_f A_c}{d_{\text{seg }1}}, T_2 = \frac{k_f A_c}{d_{\text{seg }2}}, \tag{4}$$

where k_f is the fracture permeability. A_c means the common

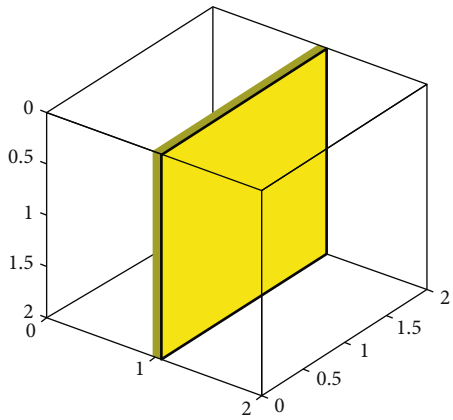

(a) Connection between the matrix grid and fracture segment

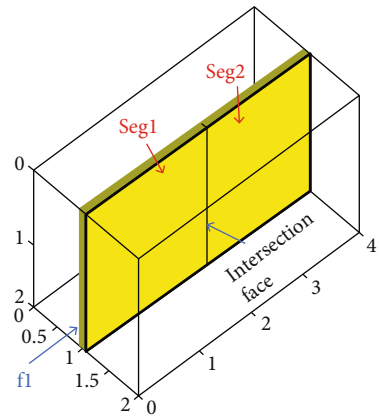

(b) Connection between fracture segments within the same fracture

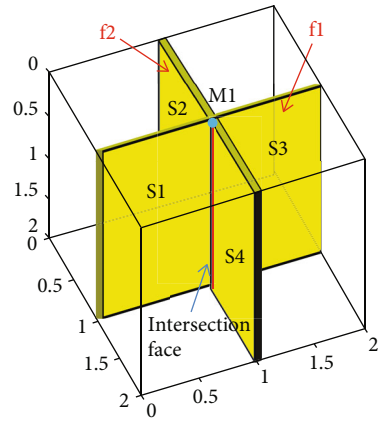

(c) Connection between different fractures

FIGURE 1: Three kinds of connections between the fracture and matrix.

plane area of two fracture segments. d_{seg1} denotes the distance from the center of fracture segment 1 to the common plane. d_{seg2} denotes the distance from the center of fracture segment 2 to the common plane.

2.1.3. Transmissibility of Connection between Different Fractures. Figure 1(c) shows the intersection between two different fractures. The transmissibility between them can be calculated by [62]

$$T_{\text{int}} = \frac{T_1 T_2}{T_1 + T_2}, \tag{5}$$

$$T_1 = \frac{k_{f1} w_{f1} L_{\text{int}}}{d_{f1}}, T_2 = \frac{k_{f2} w_{f2} L_{\text{int}}}{d_{f2}}, \tag{6}$$

where L_{int} is the length of the intersection line. k_{f1} and k_{f2} represent the permeability of fracture 1 and fracture 2, respectively. d_{f1} and d_{f2} denote the weighted average distance from the intersection line to the fracture 1 and fracture 2, respectively. w_{f1} and w_{f2} are the fracture aperture of fracture 1 and fracture 2, respectively.

2.2. Well Index. The well index in EDFM can be calculated through the effective well index of the fracture segment intersecting with the horizontal wellbore, as shown in [62]

$$WI_f = \frac{2\pi k_f w_f}{\ln\left(r_e / r_w\right)}, \tag{7}$$

$$r_e = 0.14\sqrt{L^2 + W^2}, \tag{8}$$

where k_f and w_f are the permeability and aperture of the fracture. r_e and r_w represent the supply radius and well radius. L means the fracture length, and W is the fracture height.

After the calculation of transmissibility of different NNCs and the well index, the EDFM model can be coupled with commercial reservoir simulators for numerical simulation efficiently [64].

3. Well Interference Modelling

3.1. Model Design. Based on the well distribution and fracture features in shale gas reservoirs, six physical models are designed to analyze the effect of well interference on production performance. The distribution of horizontal well, hydraulic fractures, and natural fractures of two MFHWs are presented in Figure 2.

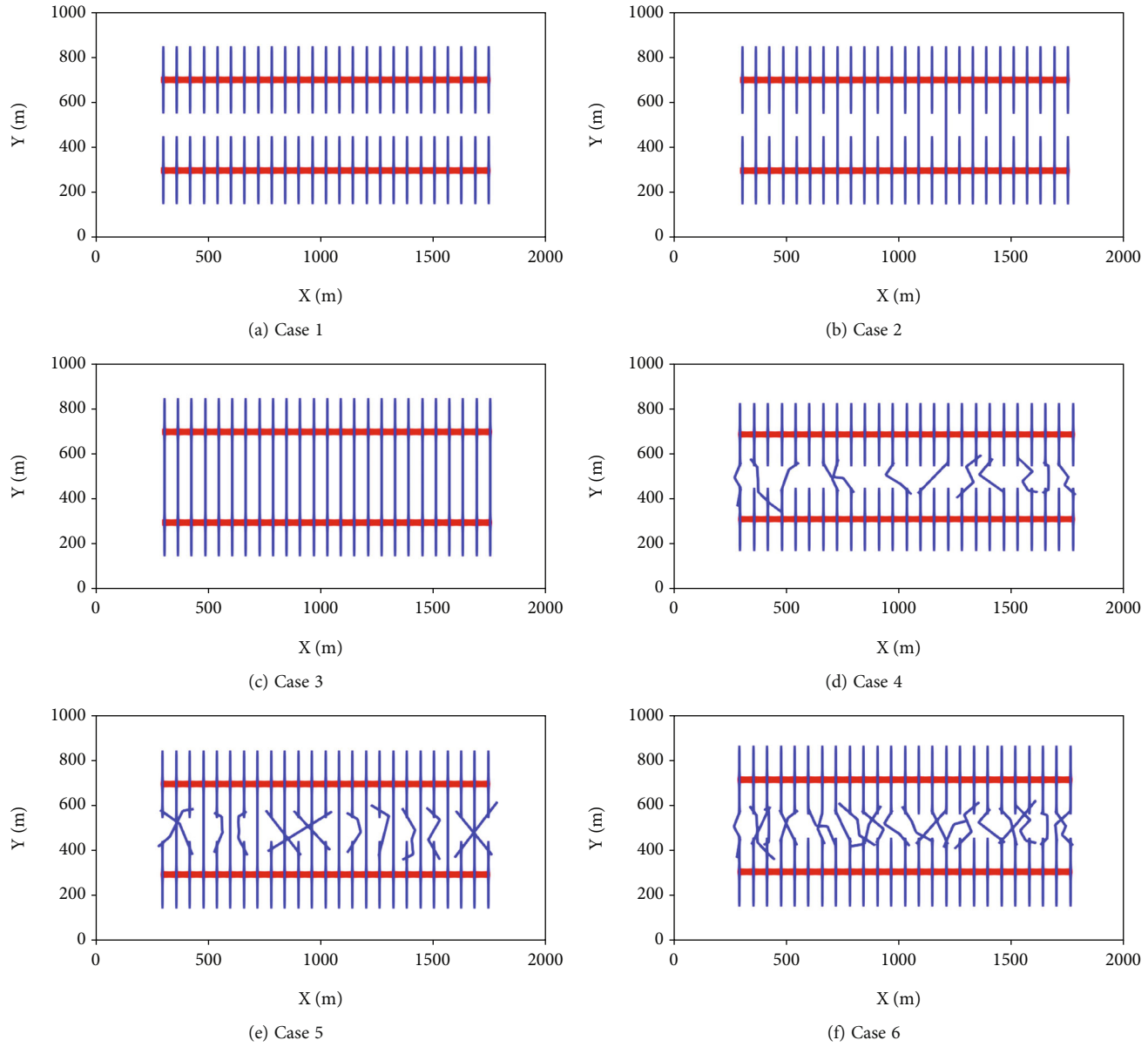

Figure 2: Distribution of horizontal wells and hydraulic fractures as well as natural fractures. (a) Two horizontal wells are not directly connected. (b) Two horizontal wells are connected through partial hydraulic fractures. (c) Two horizontal wells are connected through all hydraulic fractures. (d) Two horizontal wells are connected through partial natural fractures. (e) Two horizontal wells are connected through both hydraulic fractures and natural fractures. (f) Two horizontal wells are connected through numerous natural fractures.

Case 1. Two horizontal wells are not directly connected (see Figure 2(a)). Pressure interference is dominated through matrix.

Case 2. Two horizontal wells are connected through 50% hydraulic fractures (see Figure 2(b)). And well interference is composed of fracturing interference and pressure interference through hydraulic fractures and matrix.

Case 3. Two horizontal wells are connected through all hydraulic fractures (see Figure 2(c)). And well interference is composed of fracturing interference and pressure interference through all hydraulic fractures and matrix.

Case 4. Two horizontal wells are connected through partial natural fractures (see Figure 2(d)). And well interference is composed of fracturing interference and pressure interference through natural fractures and matrix.

Case 5. Two horizontal wells are connected through both hydraulic fractures and natural fractures (see Figure 2(e)). Well interference is caused by fracturing interference and pressure interference through hydraulic, natural fractures, and matrix.

Case 6. Two horizontal wells are connected through lots of natural fractures (see Figure 2(f)). The well interference is

Table 1: Basic parameters of formation, horizontal wells, and fractures.

Parameters	Value	Parameters	Value
Formation permeability	0.0001 mD	Well length	1460 m
Porosity	0.06	Number of hydraulic fractures	50
Formation height	35 m	Hydraulic fracture conductivity	20 mD m
Compressibility coefficient	$1.0e-7$ 1/kPa	Natural fracture conductivity	2 mD m
Initial pressure	60000 kPa	Well radius	0.1 m

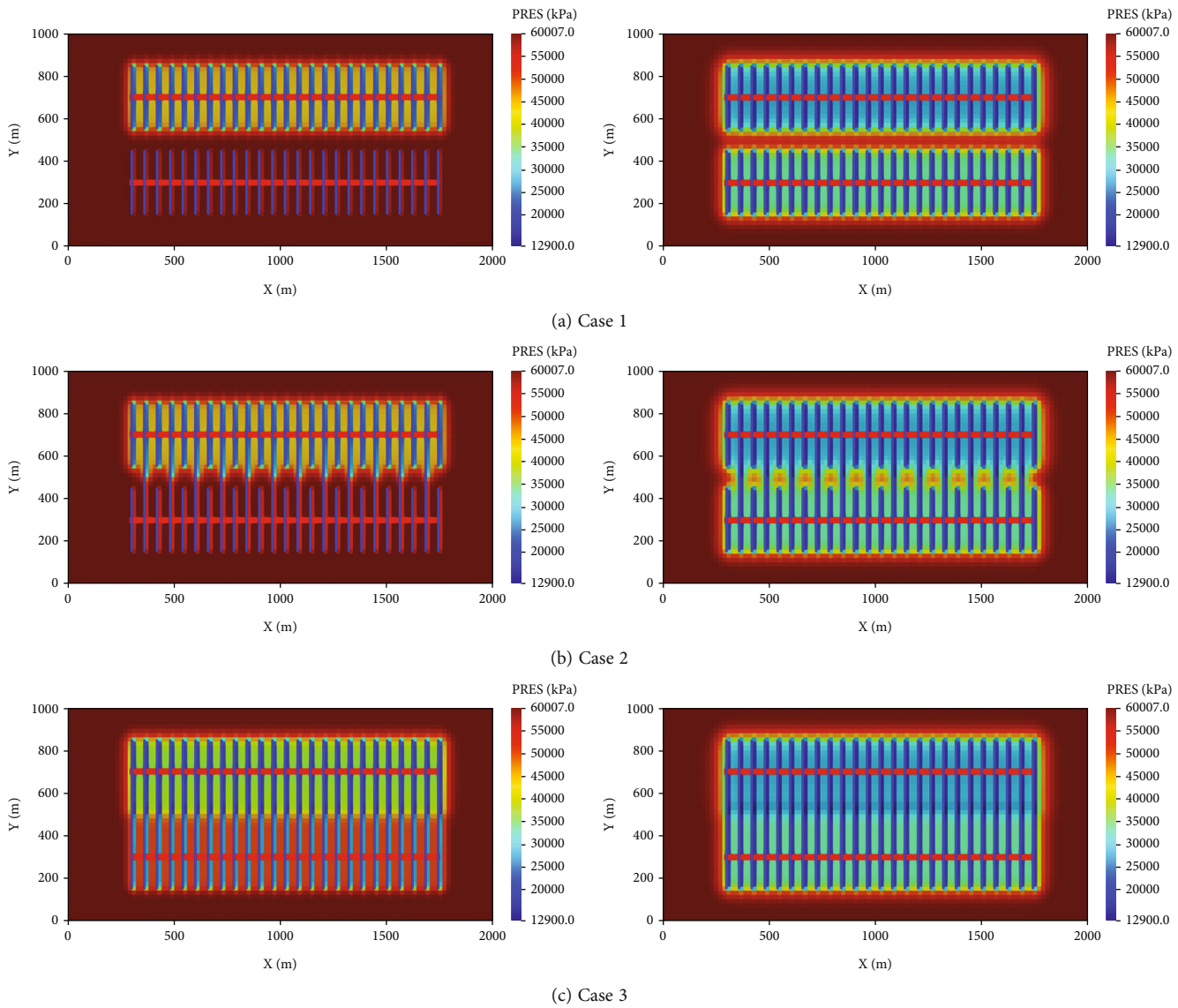

(a) Case 1

(b) Case 2

(c) Case 3

Figure 3: Pressure distribution of two MFHWs considering only hydraulic fractures in different time steps. (a) Two horizontal wells are not directly connected. (b) Two horizontal wells are connected through partial hydraulic fractures. (c) Two horizontal wells are connected through all hydraulic fractures.

caused by fracturing interference and pressure interference through lots of natural fractures and matrix.

The basic parameters of shale gas reservoirs, horizontal wells, and fractures can be seen in Table 1.

3.2. Pressure Distribution. To consider the effect of fracturing fluid on gas production, fluids are injected into the parent well from Jan 2, 2020 to Jan 20, 2020, and the well was further shut in for 11 days. From Feb 1, 2020, the parent well was put into production. The designed gas production is 250000 m^3/d and the minimum bottom-hole pressure (BHP) is set as 5 MPa. After about two years, the child well was fractured beginning from Jan 1, 2022 to Jan 20, 2022. The child well began to produce gas and water from Feb 1,

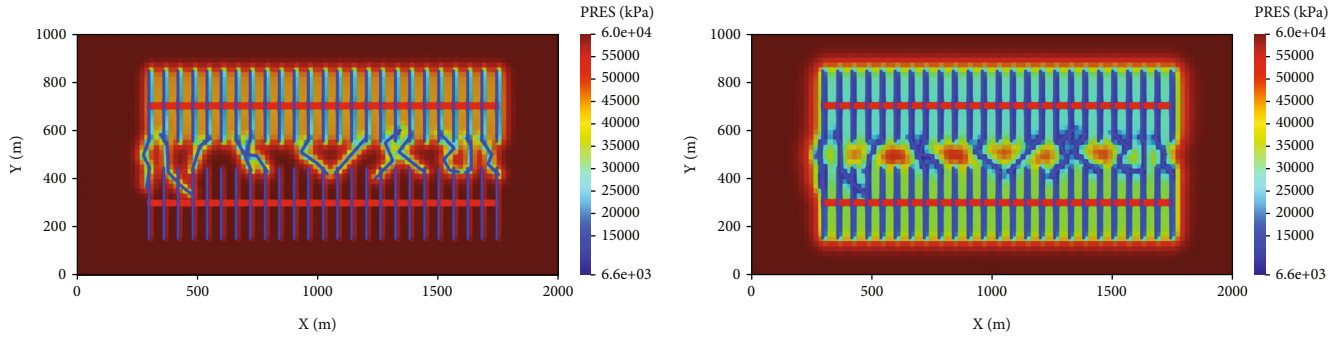

(a) Case 4

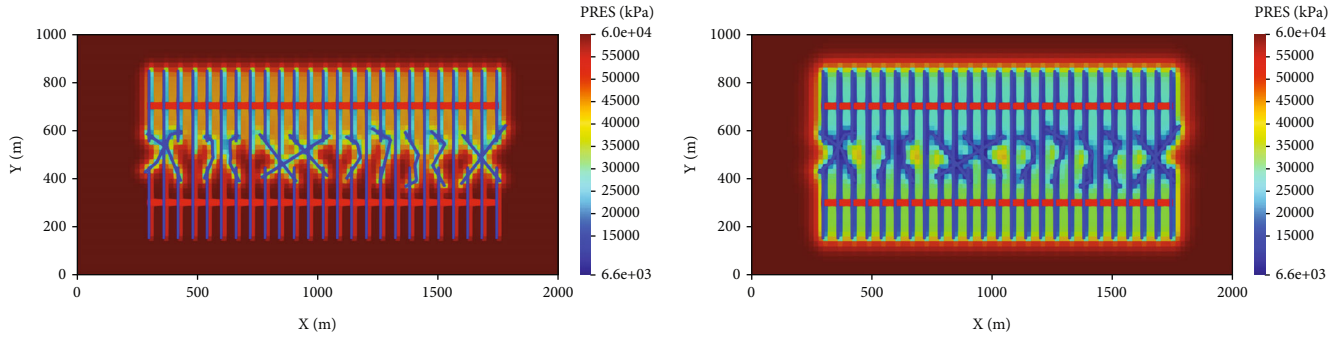

(b) Case 5

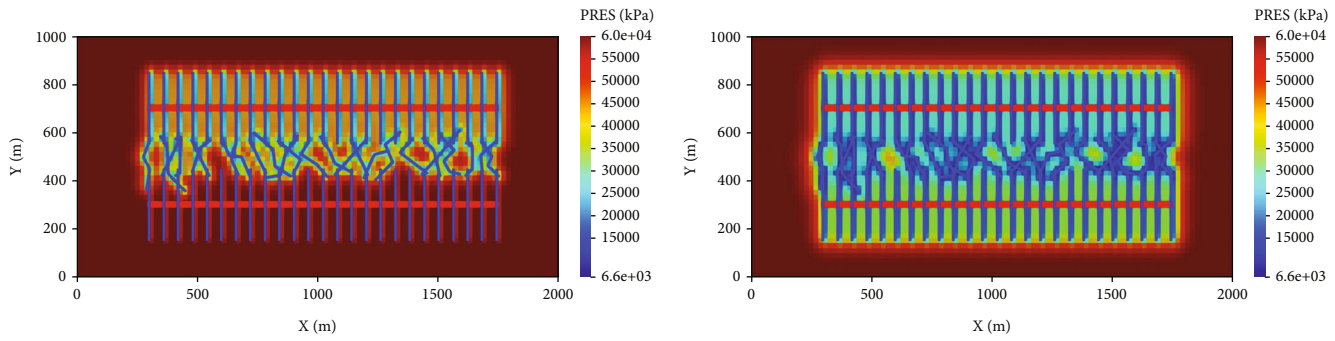

(c) Case 6

Figure 4: Pressure distribution of two MFHWs considering both hydraulic fractures and natural fractures. (a) Two horizontal wells are connected through partial natural fractures. (b) Two horizontal wells are connected through both hydraulic fractures and natural fractures. (c) Two horizontal wells are connected through numerous natural fractures.

2022. For the child well, the gas production is also set as 250000 m^3/d and the minimum bottom-hole pressure (BHP) is 5 MPa.

To compare the well interference of different cases, the pressure distribution in different time steps (Mar 2022 and Dec 2025) of two MFHWs considering only hydraulic fractures (Cases 1 to 3) are obtained as shown in Figure 3. In the early period, the difference of pressure distribution between Case 1 and Case 2 is not obvious as shown in Figures 3(a) and 3(b). However, the difference gradually becomes bigger since the well interference becomes stronger when two horizontal wells are connected with partial hydraulic fractures. If the two wells are totally connected through all hydraulic fractures (see Figure 3(c)), the well interference is obvious and the impact of well interference on the pressure distribution is significant. The pressure depletion is obvious when the well communication degree becomes higher, which can provide guidance for well spacing optimization.

Except for the effect of hydraulic fractures on well interference and pressure distribution, the impact of natural fractures also needs to be investigated. The pressure distribution of two MFHWs considering hydraulic fractures and natural fractures under three kinds of well connection conditions are shown in Figure 4. Firstly, the pressure distribution of Case 4 (see Figure 4(a)) is quite different with Case 1 (see Figures 3 (a)). It indicates that well interference is obvious when two horizontal wells are directly connected through hydraulic fractures or natural fractures. In addition, the impact of natural fractures on pressure distribution is relatively weaker than hydraulic fractures especially for the late period (see Figures 4(b) and 4(c)). However, it is hard to quantitatively evaluate the well interference and its impact on gas production only based on the pressure distribution.

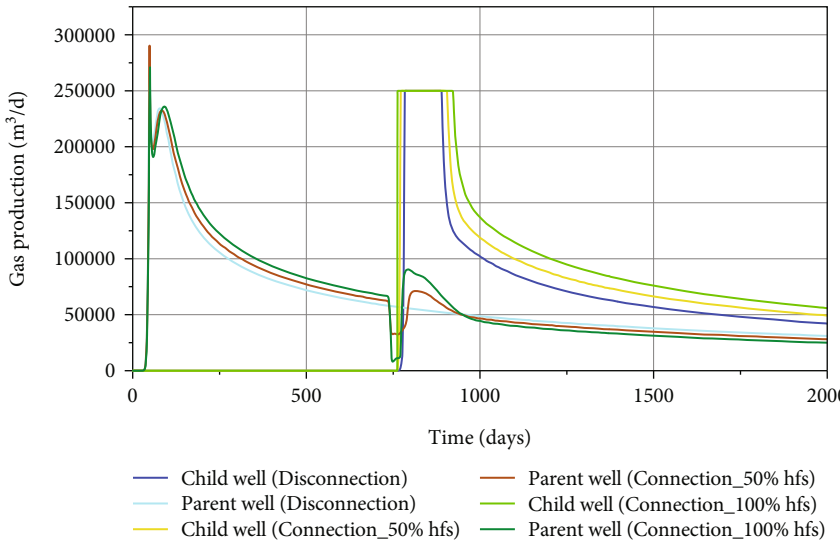

FIGURE 5: Production curves of two MFHWs considering only hydraulic fractures.

4. Well Interference Analysis

Type cures are developed to further quantitatively analyze the well interference, including the log-log type curve and Blasingame type curve. The feature on log-log type curve and Blasingame type curve under different well connections are identified to evaluate well interference.

4.1. Log-Log Type Curve. The log-log type curve is composed of the rate normalized pressure integral and rate normalized pressure integral derivative. The rate normalized pressure integral can be defined as

$$P_{\mathrm{rni}} = \frac{1}{t_e}\int_0^{t_e} \frac{p_i - p_{wf}(\tau)}{q(\tau)}\,d\tau. \tag{9}$$

On the basis of Equation (9), the rate normalized pressure integral derivative can be obtained shown as Equation (10).

$$P_{\mathrm{rniD}} = \frac{\partial}{\partial \ln t_e}\left[\frac{1}{t_e}\int_0^{t_e} \frac{p_i - p_{wf}(\tau)}{q(\tau)}\,d\tau\right], \tag{10}$$

where p_{rni} and p_{rniD} represent the rate normalized pressure integral and its derivative, respectively. P_i is the initial formation pressure. P_{wf} is the bottom-hole pressure. q is the gas production. t_e is the equivalent time, and $t_e = Q(t)/(2q(t))$.

4.2. Blasingame Type Curve. The Blasingame type curves are proposed to handle the production data under changeable pressure and production rate [65]. It is composed of pressure normalized rate, pressure normalized rate integral, and pressure normalized rate integral derivative curves.

The pressure normalized rate is defined as

$$R_{\mathrm{pn}} = \frac{q(\tau)}{p_i - p_{wf}(\tau)}. \tag{11}$$

The pressure normalized rate integral can be calculated

$$R_{\mathrm{pni}} = \frac{1}{t_e}\int_0^{t_e} \frac{q(\tau)}{p_i - p_{wf}(\tau)}\,d\tau. \tag{12}$$

Based on Equation (12), the pressure normalized rate integral be expressed as

$$R_{\mathrm{pniD}} = \frac{\partial}{\partial \ln t_c}\left[\frac{1}{t_c}\int_0^{t_c} \frac{q(\tau)}{p_i - p_{wf}(\tau)}\,d\tau\right], \tag{13}$$

where R_{pn}, R_{pni}, and R_{pniD} represent the pressure normalized rate, pressure normalized rate integral, and its derivative, respectively. P_i is the initial formation pressure. t_c means the material balanced time, and $t_c = Q(t)/q(t)$.

4.3. Well Interference Type Curve. To compare the impact of hydraulic fractures and natural fractures, we separate the six cases into two groups. The first group consists of Cases 1, 2, and 3. The second group is composed of Case 1, 4, 5, and 6.

Firstly, the production data needs to be analyzed and compared. The production curves of two MFHWs considering only hydraulic fractures under three kinds of well connection conditions (Cases 1 to 3) are shown in Figure 5. After the wells are connected through hydraulic fractures, the gas production of the parent well decreases rapidly and the water production increases quickly. Bigger decline of gas production for the parent well can be identified with the increase of well communication degree (e.g., from Case 2 to Case 3). Although it begins to recover in the later stage, it is still lower than that of parent wells with lower well communication degree. However, the gas production of child well shows the opposite characteristics. Higher communication degree between wells through hydraulic fractures results in the stimulation area or degree for the child well so that the gas production is slightly higher than that with lower communication degree or even disconnection. It indicates that

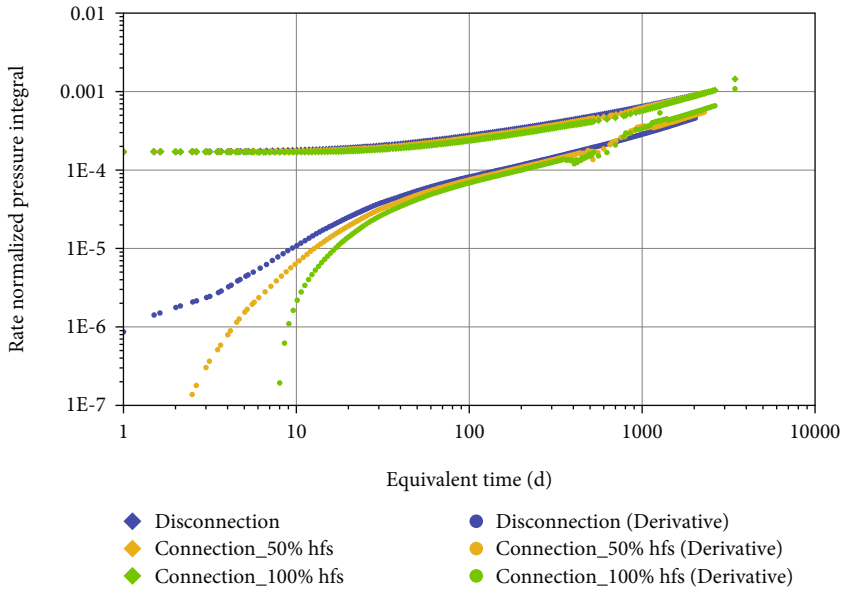

Figure 6: Log-log type curves of different well connection conditions considering only hydraulic fractures.

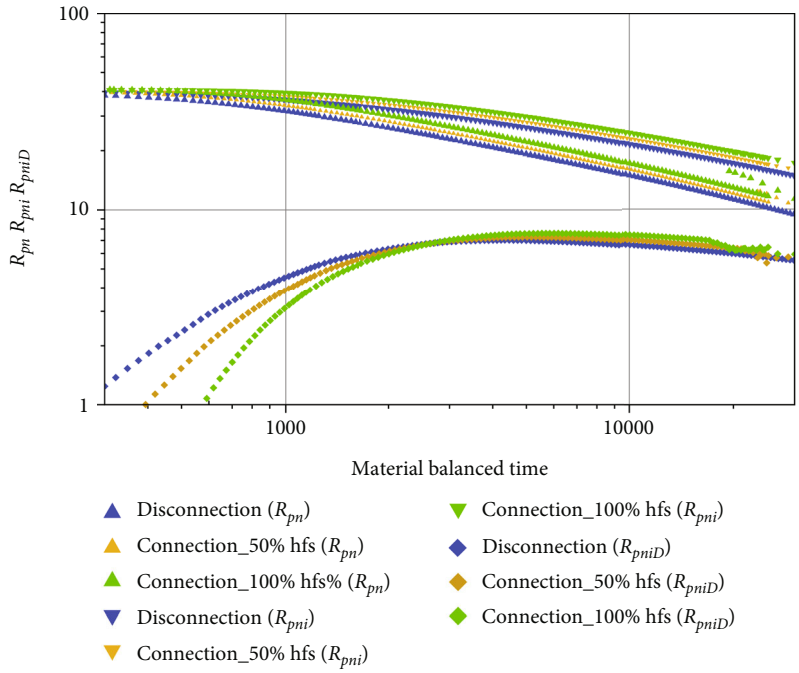

Figure 7: Blasingame type curves of different well connection conditions considering only hydraulic fractures.

well interference caused by hydraulic fractures mainly reduce the gas production of the parent well while the gas production of child well can be increased owing to the larger equivalent stimulation area and degree.

Then, the production and pressure data can be processed by using the Equations (9) and (10). The log-log type curves are generated for the MFHWs considering only hydraulic fractures under three different well connection conditions (Cases 1 to 3), shown in Figure 6. Obvious differences can be found from early to late periods in the log-log type curves when two horizontal wells are connected with hydraulic fractures (Cases 2 and 3) or two wells are not directly connected with hydraulic factures (Case 1). Especially, the distinctions during early period are more obvious. The rate normalized pressure integral derivative drops a lot with the increase of well connectivity, while it becomes larger under late period with the increase of well connectivity. Therefore, well interference can be identified using the log-log type curves.

Furthermore, the Blasingame type curves can also be obtained using the Equations (11) and (13) based on the production and pressure data. Figure 7 shows the Blasingame type

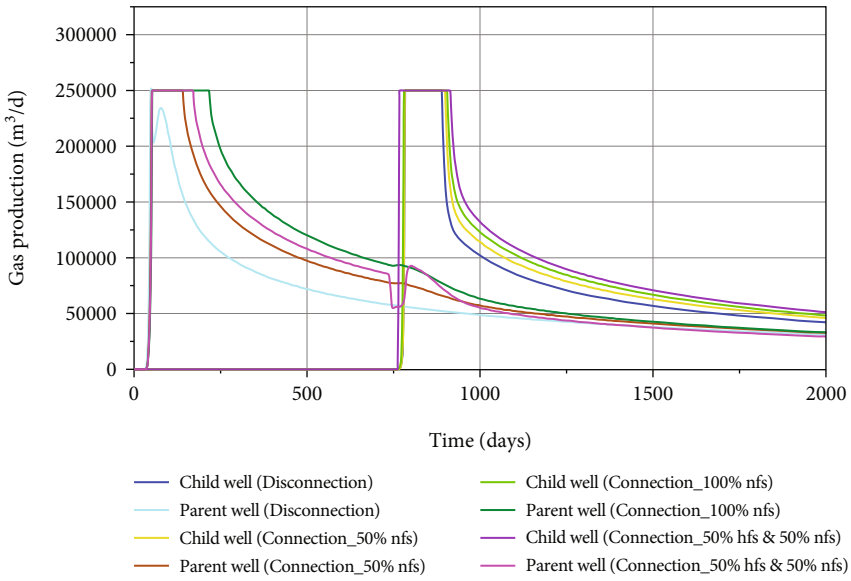

Figure 8: Production curves of two MFHWs considering both hydraulic fractures and natural fractures.

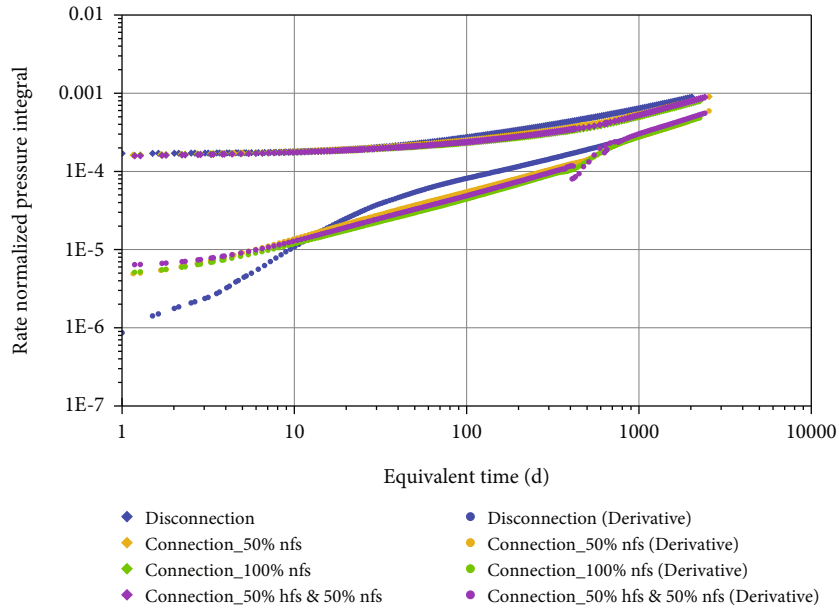

Figure 9: Log-log type curves of different well connection conditions considering both hydraulic fractures and natural fractures.

curves for the MFHWs considering only hydraulic fractures under three different well connection conditions (Cases 1 to 3). Distinctions can be observed on the type curves among different well connection conditions by the combination of pressure normalized rate, pressure normalized rate integral, and pressure normalized rate integral derivative, especially during early and late periods. When two wells are communicated directly through hydraulic fractures, the pressure normalized rate integral derivative drops a lot during the early stage with the increase of well connectivity, while it moves up under late period with the increase of well connectivity. The differences during the late period on the Blasingame type curves among three cases are bigger than that on the log-log type curves, while the features during early period on the log-log type curves are clearer. Thus, the well interference of shale gas reservoirs can be identified by the combination of the log-log and Blasingame type curves.

In this part, the impact of natural fractures on the production data and type curves will be analyzed. The production curves of two MFHWs considering both hydraulic fractures and natural fractures under three kinds of well connection conditions (Cases 4 to 6) are shown in Figure 8. Case 1 was included in this part to show the comparison. Compared to Case 1, more fractures are added in to Cases 4 to 6 so that the gas production is improved owing to bigger simulated area. When the fracturing interference

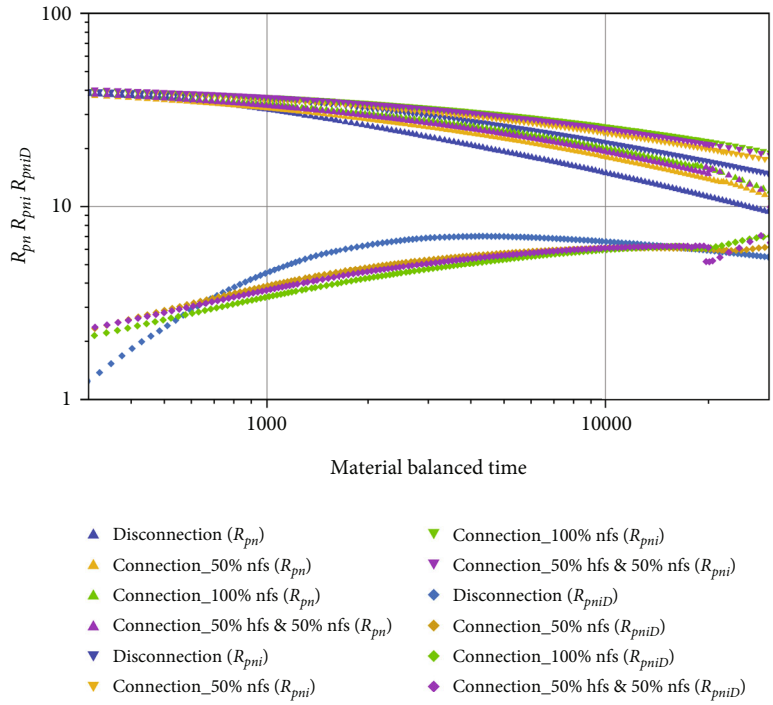

Figure 10: Blasingame type curves of different well connection conditions considering both hydraulic fractures and natural fractures.

occurs, the gas production of the parent well decreases due to the impact of fracturing fluids from the child well. Different from Figure 5, the decline degree of gas production is minor when child well is connecting parent well only through natural fractures (Cases 4 and 6). But, if two wells are communicated with natural and hydraulic fractures, the gas production of the parent well decline a lot (Case 5). We can conclude that well interference caused by natural fractures is much weaker compared to hydraulic fractures.

To identify the impact of well interference caused by natural fractures, log-log type curves are generated as shown in Figure 9. On the one hand, differences can be observed between Case 1 and Cases 4 to 6, especially on the rate normalized pressure integral derivative curves. On the other hand, the distinctions are minor if the parent well and child well are communicated with only natural fractures (Cases 4 and 6). Additionally, the impact of fracturing interference caused by hydraulic fractures or numerous natural fractures can be identified using the rate normalized pressure integral derivative curve (Case 5 and 6).

The feature of fracturing interference is not obvious enough on the log-log type curves so that the Blasingame type curves are developed based on the production and pressure data of Cases 1, 4, 5, and 6 (see Figure 10). It is obvious that major differences during early, middle, and late periods can be found on the Blasingame type curves under different well communication degrees. And the signal of fracturing interference caused by the natural fractures is more obvious.

5. Conclusions

This paper focuses on the well interference analysis of shale gas wells. EDFM technology is introduced to deal with the hydraulic fractures and natural fractures as well as model the well interference caused by hydraulic and natural fractures.

(1) After the wells are communicated through hydraulic fractures, the gas production of the parent well declines a lot due to the fracturing fluids from the child well. However, if two wells are connected only through natural fractures, the decline degree of gas production is much minor. Well interference caused by natural fractures is much weaker compared to hydraulic fractures

(2) For wells connected through hydraulic fractures, the differences during the late period on the Blasingame type curves are clearer than that on the log-log type curves, while the features during early period on the log-log type curves are easier to distinguish

(3) For wells connected through only natural fractures, the distinctions are minor if the parent well and child well are communicated with only natural fractures, the signal of fracturing interference caused by the natural fractures are more obvious on the Blasingame type curves

Thus, the well interference of shale gas reservoirs can be identified by the combination of log-log and Blasingame type curves. This work can be helpful for understanding the well interference feature and its impact on shale gas production.

Data Availability

The data used to support the findings of this study are included in the article.

Conflicts of Interest

The author declares that there is no conflict of interest regarding the publication of this paper.

Acknowledgments

This work was financially supported by the Chuanqing scientific project (CQXN-2020-09).

References

[1] F. Javadpour, D. Fisher, and M. Unsworth, "Nanoscale gas flow in shale gas sediments," *Journal of Canadian Petroleum Technology*, vol. 46, no. 10, 2007.

[2] D. J. Ross and R. M. Bustin, "The importance of shale composition and pore structure upon gas storage potential of shale gas reservoirs," *Marine and Petroleum Geology*, vol. 26, no. 6, pp. 916–927, 2009.

[3] K. Liu, L. Wang, M. Ostadhassan, J. Zou, B. Bubach, and R. Rezaee, "Nanopore structure comparison between shale oil and shale gas: examples from the Bakken and Longmaxi Formations," *Petroleum Science*, vol. 16, no. 1, pp. 77–93, 2019.

[4] X. Zhao, L. Zhou, and X. Pu, "Formation conditions and enrichment model of retained petroleum in lacustrine shale: a case study of the Paleogene in Huanghua depression, Bohai Bay Basin, China," *Petroleum Exploration and Development*, vol. 47, no. 5, pp. 916–930, 2020.

[5] L. Huang, W. Zhou, H. Xu, L. Wang, J. Zou, and Q. Zhou, "Dynamic fluid states in organic-inorganic nanocomposite: implications for shale gas recovery and CO_2 sequestration," *Chemical Engineering Journal*, vol. 411, p. 128423, 2021.

[6] J. Liu, L. Xie, B. He, P. Zhao, and H. Y. Ding, "Performance of free gases during the recovery enhancement of shale gas by CO2 injection: a case study on the depleted Wufeng–Longmaxi shale in northeastern Sichuan Basin, China," *Petroleum Science*, vol. 18, no. 2, pp. 530–545, 2021.

[7] D. Rahm, "Regulating hydraulic fracturing in shale gas plays: the case of Texas," *Energy Policy*, vol. 39, no. 5, pp. 2974–2981, 2011.

[8] M. B. Seales, T. Ertekin, and J. Yilin Wang, "Recovery efficiency in hydraulically fractured shale gas reservoirs," *Journal of Energy Resources Technology*, vol. 139, no. 4, article 042901, 2017.

[9] J. Xie, J. Tang, R. Yong et al., "A 3-D hydraulic fracture propagation model applied for shale gas reservoirs with multiple bedding planes," *Engineering Fracture Mechanics*, vol. 228, p. 106872, 2020.

[10] Y. He, J. Qin, S. Cheng, and J. Chen, "Estimation of fracture production and water breakthrough locations of multi- stage fractured horizontal wells combining pressure-transient analysis and electrical resistance tomography," *Journal of Petroleum Science and Engineering*, vol. 194, p. 107479, 2020.

[11] C. Ou, C. Liang, Z. Li, L. Luo, and X. Yang, "3D Visualization of Hydraulic Fractures Using Micro-Seismic Monitoring: Methodology and Application," *Petroleum*, vol. 8, no. 1, pp. 92–101, 2022.

[12] J. Zhao, L. Ren, and T. Jiang, "Ten years of gas shale fracturing in China: review and prospect," *Natural Gas Industry*, vol. 41, no. 8, pp. 121–142, 2021.

[13] S. Mao, Z. Zhang, T. Chun, and K. Wu, "Field-scale numerical investigation of proppant transport among multi-cluster hydraulic fractures," *SPE Journal*, vol. 26, no. 1, pp. 307–323, 2021.

[14] Y. Duan, H. Wang, M. Wei, L. Tan, and T. Yue, "Application of ARIMA-RTS Optimal Smoothing Algorithm in Gas Well Production Prediction," *Petroleum*, 2021.

[15] A. Ajani and M. Kelkar, "Interference study in shale plays," in *SPE Hydraulic Fracturing Technology Conference*, The Woodlands, Texas, USA, February 2012.

[16] A. Morales, K. Zhang, K. Gakhar et al., "Advanced modeling of interwell fracturing interference: an Eagle Ford shale oil study-refracturing," in *SPE Hydraulic Fracturing Technology Conference*, The Woodlands, Texas, USA, February 2016.

[17] B. Lin, H. Meng, J. Pan, and S. Chen, "Porothermoelastic response of an oil sand formation subjected to injection and micro-fracturing in horizontal wells," *Petroleum Science*, vol. 17, no. 3, pp. 687–700, 2020.

[18] H. Lawal, G. Jackson, N. Abolo, and C. Flores, "A novel approach to modeling and forecasting frac hits in shale gas wells," in *EAGE Annual Conference and Exhibition incorporating SPE Europec*, London, UK, June 2013.

[19] P. Moradi and D. Angus, "Modeling frac-hits using dynamic microseismicity-constrained enhanced fracture regions," in *SPE/AAPG/SEG Unconventional Resources Technology Conference*, Denver, Colorado, USA, July 2019.

[20] X. Guo, K. Wu, C. An, J. Tang, and J. Killough, "Numerical investigation of effects of subsequent parent well injection on interwell fracturing interference using reservoir-geomechanics-fracturing modeling," *SPE Journal*, vol. 24, no. 4, pp. 1884–1902, 2019.

[21] S. D. Mohaghegh, "Frac-hit dynamic modeling using artificial intelligence and machine learning," in *SPE/AAPG/SEG Unconventional Resources Technology Conference, Virtual*, July 2020.

[22] A. Khodabakhshnejad, "Impact of frac hits on production performance- a case study in Marcellus Shale," in *SPE Western Regional Meeting*, San Jose, California, USA, April 2019.

[23] R. Esquivel and T. A. Blasingame, "Optimizing the development of the Haynesville shale - lessons learned from well-to-well hydraulic fracture interference," in *SPE/AAPG/SEG Unconventional Resources Technology Conference*, Austin, Texas, USA, July 2017.

[24] X. Guo, K. Wu, J. Killough, and J. Tang, "Understanding the mechanism of interwell fracturing interference with reservoir/geomechanics/fracturing modeling in Eagle Ford Shale," *SPE Reservoir Evaluation and Engineering*, vol. 22, no. 3, pp. 842–860, 2019.

[25] Y. He, J. Guo, Y. Tang et al., "Interwell fracturing interference evaluation of multi-well pads in shale gas reservoirs: a case study in WY Basin," in *SPE annual Technical Conference and Exhibition, Virtual*, October 2020.

[26] C. Sardinha, C. Petr, J. Lehmann, and J. Pyecroft, "Determining interwell connectivity and reservoir complexity through frac pressure hits and production interference analysis," in *SPE/CSUR Unconventional Resources Conference–Canada*, Calgary, Alberta, Canada, September 2014.

[27] I. Gupta, C. Rai, D. Devegowda, and C. Sondergeld, "Haynesville shale: predicting long-term production and residual analysis to identify well intereference and frac hits," in *SPE Oklahoma City Oil and Gas Symposium*, Oklahoma City, Oklahoma, USA, April 2019.

[28] O. M. Molina, "Analytical model to estimate the fraction of frac hits in multi-well pads," in *SPE/AAPG/SEG Unconventional Resources Technology Conference*, Denver, Colorado, USA, July 2019.

[29] A. Kumar, P. Seth, K. Shrivastava, R. Manchanda, and M. M. Sharma, "Integrated analysis of tracer and pressure-interference tests to identify well interference," *SPE Journal*, vol. 25, no. 4, pp. 1623–1635, 2020.

[30] A. Khodabakhshnejad, Y. Aimene, N. Mistry, A. Bachir, and A. Ouenes, "A fast method to forecast shale pressure depletion and well performance using geomechanical constraints - application to poro-elasticity modeling to predict mid and far field frac hits at an Eagle Ford and Wolfcamp Well," in *SPE Eastern Regional Meeting*, Lexington, Kentucky, USA, October 2017.

[31] S. Pathak, R. Tibbles, A. Bohra, S. Tiwari, P. Godiyal, and A. Deo, "Evaluation of frac hit risks in Aishwarya Barmer-Hill field development utilising GIS platform," in *SPE Asia Pacific oil and gas conference and exhibition*, Brisbane, Australia, October 2018.

[32] R. D. Magneres, M. Castello, F. Bertoldi, and M. Griffin, "Vaca Muerta frac-hit occurrence and magnitude forecast methodology," in *SPE/AAPG/SEG Latin America Unconventional Resources Technology Conference, Virtual*, November 2020.

[33] R. Cao, R. Li, A. Girardi, N. Chowdhury, and C. Chen, "Well interference and optimum well spacing for Wolfcamp development at Permian Basin," in *SPE/AAPG/SEG Unconventional Resources Technology Conference*, Austin, Texas, USA, July 2017.

[34] Y. Zhao, N. Li, J. Yang, and S. Cheng, "Optimization of deep shale gas well spacing based on geology-engineering integration: a case study of Weirong shale gas field," *Petroleum Reservoir Evaluation and Development*, vol. 11, no. 3, pp. 340–347, 2021.

[35] R. Manchanda, J. Hwang, P. Bhardwaj, M. M. Sharma, M. Maguire, and J. Greenwald, "Strategies for improving the performance of child wells in the permian basin," in *SPE/AAPG/SEG unconventional resources technology conference*, Houston, Texas, USA, July 2018.

[36] A. Rangriz Shokri, R. J. Chalaturnyk, and D. Bearinger, "Deployment of pressure hit catalogues to optimize multi-stage hydraulic stimulation treatments and future re-fracturing designs of horizontal Wells in Horn River Shale Basin," in *SPE annual Technical Conference and Exhibition*, Calgary, Alberta, Canada, September 2019.

[37] K. Vidma, P. Abivin, D. Fox et al., "Fracture geometry control technology prevents well interference in the Bakken," in *SPE Hydraulic Fracturing Technology Conference and Exhibition*, The Woodlands, Texas, USA, February 2019.

[38] M. Paryani, R. Smaoui, S. Poludasu et al., "Adaptive fracturing to avoid frac hits and interference: a Wolfcamp shale case study," in *SPE Unconventional Resources Conference*, Calgary, Alberta, Canada, February 2017.

[39] S. Zheng, R. Manchanda, D. Gala, and M. Sharma, "Pre-loading depleted parent wells to avoid frac-hits: some important design considerations," in *SPE Annual Technical Conference and Exhibition*, Calgary, Alberta, Canada, September 2019.

[40] D. P. Gala, R. Manchanda, and M. M. Sharma, "Modeling of fluid injection in depleted parent wells to minimize damage due to frac-hits," in *SPE/AAPG/SEG Unconventional Resources Technology Conference*, Houston, Texas, USA, July 2018.

[41] T. Whitfield, M. H. Watkins, and L. J. Dickinson, "Pre-loads: successful mitigation of damaging frac hits in the Eagle Ford," in *SPE Annual Technical Conference and Exhibition*, Dallas, Texas, USA, September 2018.

[42] G. E. King, M. F. Rainbolt, and C. Swanson, "Frac hit induced production losses: evaluating root causes, damage location, possible prevention methods and success of remedial treatments," in *SPE Annual Technical Conference and Exhibition*, San Antonio, Texas, USA, October 2017.

[43] C. Swanson, W. A. Hill, G. Nilson et al., "Post-frac-hit mitigation and well remediation of Woodford horizontal wells with solvent/surfactant chemistry blend," in *SPE/AAPG/SEG Unconventional Resources Technology Conference*, Houston, Texas, USA, July 2018.

[44] M. F. Rainbolt and J. Esco, "Frac hit induced production losses: evaluating root causes, damage location, possible prevention methods and success of remediation treatments, part II," in *SPE Hydraulic Fracturing Technology Conference and Exhibition*, The Woodlands, Texas, USA, January 2018.

[45] P. A. Bommer and M. A. Bayne, "Active well defense in the Bakken: case study of a ten-well frac defense project, Mckenzie county, ND," in *SPE hydraulic fracturing technology conference and exhibition*, The Woodlands, Texas, USA, January 2018.

[46] D. C. Johnson, B. B. Yeager, C. D. Roberts, and B. W. Fowler, "Offset fracture events made simple: an operator's collaborative approach to observe parent child interactions, measure frac hit severity and test mitigation strategies," in *SPE Hydraulic Fracturing Technology Conference and Exhibition*, The Woodlands, Texas, USA, February 2020.

[47] C. L. Cipolla, E. Lolon, J. Erdle, and V. S. Tathed, "Modeling well performance in shale-gas reservoirs," *SPE/EAGE Reservoir Characterization and Simulation Conference*, 2009, Abu Dhabi, UAE, October 2009, 2009.

[48] A. Mhiri, T. A. Blasingame, and G. J. Moridis, "Stochastic modeling of a fracture network in a hydraulically fractured shale-gas reservoir," in *SPE Annual Technical Conference and Exhibition*, Houston, Texas, USA, September 2015.

[49] Y. Wu, L. Cheng, J. Killough et al., "Integrated characterization of the fracture network in fractured shale gas reservoirs–stochastic fracture modeling, simulation and assisted history matching," *Journal of Petroleum Science and Engineering*, vol. 205, article 108886, 2021.

[50] Y. Xu and K. Sepehrnoori, "Development of an embedded discrete fracture model for field-scale reservoir simulation with complex corner-point grids," *SPE Journal*, vol. 24, no. 4, pp. 1552–1575, 2019.

[51] M. X. Fiallos, W. Yu, R. Ganjdanesh et al., "Modeling interwell interference due to complex fracture hits in eagle ford using EDFM," in *International Petroleum Technology Conference*, Beijing, China, March 2019.

[52] W. Yu, K. Wu, M. Liu, K. Sepehrnoori, and J. Miao, "Production forecasting for shale gas reservoirs with nanopores and complex fracture geometries using an innovative non-intrusive EDFM method," in *SPE Annual Technical Conference and Exhibition*, Dallas, Texas, USA, September 2018.

[53] Y. He, Y. Qiao, J. Qin, Y. Tang, Y. Wang, and Z. Chai, "A novel method to enhance oil recovery by inter-fracture injection and production through the same multi-fractured horizontal well," *Journal of Energy Resources Technology*, vol. 144, no. 4, article 043005, 2022.

[54] M. Onur, C. Ayan, and F. J. Kuchuk, "Pressure-pressure deconvolution analysis of multi-well interference and interval pressure transient tests," in *International Petroleum Technology Conference*, Doha, Qatar, December 2009.

[55] E. Yaich, O. C. Diaz De Souza, R. A. Foster, and I. Abou-Sayed, "A methodology to quantify the impact of well interference and optimize well spacing in the Marcellus Shale," in *SPE/CSUR Unconventional Resources Conference – Canada*, Calgary, Alberta, Canada, September 2014.

[56] C. Xiao, Y. Dai, L. Tian et al., "A semianalytical methodology for pressure-transient analysis of multiwell-pad-production scheme in shale gas reservoirs, part 1: new insights into flow regimes and multiwell interference," *SPE Journal*, vol. 23, no. 3, pp. 885–905, 2018.

[57] J. Qin, Y. Xu, Y. Tang et al., "Impact of complex fracture networks on rate transient behavior of wells in unconventional reservoirs based on embedded discrete fracture model," *Journal of Energy Resources Technology*, vol. 144, no. 8, article 083007, 2022.

[58] H. Chu, X. Liao, C. Wei, and J. Lee, "Rate/pressure transient analysis of a variable bottom hole pressure multi-well horizontal pad with well interference," in *SPE Annual Technical Conference and Exhibition*, Dubai, UAE, September 2021.

[59] Y. He, Y. Xu, Y. Tang, Y. Qiao, W. Yu, and K. Sepehrnoori, "Multi-phase rate transient behaviors of the multi-fractured horizontal well with complex fracture networks," *Journal of Energy Resources Technology*, vol. 144, no. 4, article 043006, 2022.

[60] Y. Xu, *Implementation and application of the embedded discrete fracture model (EDFM) for reservoir simulation in fractured reservoirs*, Doctoral dissertation. The University of Texas at Austin, Texas, USA, 2015.

[61] A. Yaghoubi, "Hydraulic fracturing modeling using a discrete fracture network in the Barnett Shale," *International Journal of Rock Mechanics and Mining Sciences*, vol. 119, pp. 98–108, 2019.

[62] Y. Xu, J. Cavalcante Filho, W. Yu, and K. Sepehrnoori, "Discrete-fracture modeling of complex hydraulic-fracture geometries in reservoir simulators," *SPE Reservoir Evaluation and Engineering*, vol. 20, no. 2, pp. 403–422, 2017.

[63] Z. Chai, H. Tang, Y. He, J. Killough, and Y. Wang, "Uncertainty quantification of the fracture network with a novel fractured reservoir forward model," in *SPE Annual Technical Conference and Exhibition*, Dallas, Texas, USA, September 2018.

[64] W. Yu, K. Wu, L. Zuo, J. Miao, and K. Sepehrnoori, "Embedded discrete fracture model assisted study of gas transport mechanisms and drainage area for fractured shale gas reservoirs," in *SPE/AAPG/SEG Unconventional Resources Technology Conference*, Denver, Colorado, USA, July 2019.

[65] T. A. Blasingame, T. L. McCray, and W. J. Lee, "Decline curve analysis for variable pressure drop/variable flowrate systems," in *SPE Gas Technology Symposium*, Houston, Texas, January 1991.